A Method for Correcting Signal Aberrations in Ultrasonic Indoor Positioning

Riccardo Carotenuto *, Demetrio Iero, Massimo Merenda

Posted Date: 30 January 2024

doi: 10.20944/preprints202401.2135.v1

Keywords: acoustic signal aberration; cross-correlation aberration; ultrasonic ranging; acoustic SNR

Article

A Method for Correcting Signal Aberrations in Ultrasonic Indoor Positioning

Riccardo Carotenuto [1,*], Demetrio Iero [1,2] and Massimo Merenda [1,2]

[1] DIIES Department, University Mediterranea of Reggio Calabria, Reggio Calabria 89126, Italy; demetrio.iero@unirc.it (D.I.)
[2] HWA Srl, Spin-Off University Mediterranea of Reggio Calabria, Via R. Campi II tr. 135, Reggio Calabria 89126, Italy
* Correspondence: r.carotenuto @unirc.it; Tel.: +39-0965-1693-464

Abstract: The increasing focus on the development of positioning techniques reflects the growing interest in applications and services based on indoor positioning. Many applications necessitate precise indoor positioning or tracking of individuals and assets, leading to rapid growth in products based on these technologies in certain market sectors. Ultrasonic systems have already proven effective in achieving the desired positioning accuracy and refresh rates. The typical signal used in ultrasonic positioning systems for estimating the range between the target and reference points, specifically the linear chirp, can undergo shape aberration due to the effects of acoustic diffraction when the aperture exceeds a certain limit. The extent of the aberration is influenced by the shape and size of the transducer, as well as the angle at which the transducer is observed by the receiver. This aberration also impacts the shape of the cross-correlation, causing it to lose its characteristic easily detectable single global peak. In such instances, cross-correlation techniques yield results with a significantly higher error than anticipated. In this study, an alternative technique to global peak detection is proposed, leveraging the inherent symmetry observed in the shape of the aberrated cross-correlation. The numerical simulations, performed using the academic acoustic simulation software Field II, conducted using a typical ultrasonic chirp and ultrasonic emitter, compare the classical and the proposed range techniques in a standard office room. The results demonstrate that the proposed technique enables accurate range estimation even in the presence of severe cross-correlation shape aberrations. This allows the use of emitting transducers with a much larger aperture than that allowed by the classical cross-correlation technique. Consequently, it becomes possible to have greater acoustic power available, leading to improved Signal-to-Noise Ratio (SNR).

Keywords: acoustic signal shape aberration; cross-correlation shape aberration; ultrasonic ranging; acoustic SNR

1. Introduction

Emerging technologies like Augmented Reality (AR) and various positioning-based applications are driving the need for indoor positioning technology. Positioning systems with the ability to provide precise accuracy in indoor settings are essential for various applications, including but not limited to mall navigation, pathfinding in large hospitals or airports, automatic guidance for unmanned cleaning and maintenance vehicles, surveillance systems, and more [1–5]. Trilateration, a well-established technique, is commonly employed in accurate positioning systems for indoor use. This method relies on three (or more) range measurements between emitters placed at reference locations and a sensor to determine their distances and spatial positions with a high degree of accuracy at a relatively low cost. Ultrasonic wave-based systems have proven effective in providing accurate positioning [6–9].

The widely used ranging technique involves estimating the Time of Arrival (TOA) of a suitable ultrasonic signal. Typically, TOA is determined by identifying a specific feature in the received signal or the post-processed signal that is easily recognizable upon arrival. In certain situations, the determination of the time of arrival (TOA) often relies on pinpointing the maximum peak within the

 doi:10.20944/preprints202401.2135.v1

envelope of an ultrasonic pulse. However, despite the apparent simplicity of this method, it remains susceptible to disruptions caused by acoustic interference, leading to errors on the scale of wavelengths (centimeters), even with a high Signal-to-Noise Ratio (SNR) [9–13].

Methods employing cross-correlation, on the other hand, provide a markedly precise estimation of TOA and generally demonstrate robust resistance to acoustical disturbances [12–15]. Digital cross-correlation techniques proficiently sample and transform the received acoustical signal into the array C = S ★ T. In this context, S denotes the numerical array of received signal samples, T represents the digital reference signal stored in the sensor processor memory as a numerical array of samples, and ★ serves as the cross-correlation operator. The optimum alignment of S and T in time is discerned through the peak of the cross-correlation. The displacement between signals, or lag τ, corresponding to the cross-correlation peak (i.e., τ_{MAX}), is directly proportional to the TOA [16,17].

The precision in measuring distance, within the current spatial sampling framework—defined as the distance traversed by ultrasound during the time sample interval—can be markedly reduced compared to the ultrasonic wavelength. This enhanced accuracy is achieved by determining the TOA through the identification of the cross-correlation peak.

In practical systems, a range resolution can be achieved up to approximately one-tenth of the wavelength used. For instance, in [14], an experimental range resolution of ±1.2 mm was attained using a 15 – 40 kHz chirp, with a wavelength range of 22.86 – 8.57 mm. This was realized considering a sampling frequency of 1 MHz, resulting in a space sampling of 0.34 mm, and utilizing a sound speed of 343 m/s. In cases where the signal and noise are uncorrelated, the process of cross-correlation significantly enhances the Signal-to-Noise Ratio (SNR), commonly referred to as process gain.

Extensive research has been conducted in the past on the acoustic field produced by acoustic transducers, considering impulsive or continuous sinusoidal wave signals and varying the shape and aperture of the transducer. The exploration of closed-form solutions for the generated acoustic field has facilitated the derivation of simple approximate formulas for calculating the emission angle. These formulas depend on factors such as wavelength, aperture, and distance from the emitter, with the most recognized ones being applicable to circular apertures. In the far field, the semi-angle ϑ of the emission cone is approximately characterized by the well-established relationship [18]:

$$\sin\vartheta = 1.22\frac{\lambda}{D} \tag{1}$$

where D is the diameter or aperture of the transducer and λ is the emitted wavelength.

Furthermore, it is well-established that achieving optimal results in signal reception requires the receiver to consistently operate within the designated "emission cone" of the emitter [19]. Presently, there are no equivalent formulas applicable to signals of varying shapes, such as chirp signals. In the development of a positioning system based on ultrasonic signals, the utilization of numerical tools becomes essential to evaluate the spatial coverage of each transducer in terms of the quality (including amplitude and deformation level) of the received signal. For signals with arbitrary shapes, reliable indications cannot be derived from simplified formulas, making the use of numerical tools imperative.

In the context of the considered ultrasonic positioning systems, simulations must encompass extensive spatial domains, spanning several cubic meters, and temporal windows extending over tens of milliseconds (see, for instance, [8,9,12]). A robust numerical instrument, the academic Field II software [20,21], has demonstrated its suitability for analyzing ultrasound positioning systems. It allows simulating any shape of transducers and ultrasonic signals for both transmission and reception. Moreover, Field II has the numerical features that allow simulating the large spatial regions and time windows required in the field of ultrasonic positioning. This tool is also able to take into account the attenuation properties of the propagation medium.

In a past work [22], using Field II, it was shown that a chirp emitted by a transducer with a certain aperture, and consequently its cross-correlation, undergoes a shape aberration that increases with a larger aperture. The larger the aperture, the narrower the useful emission cone within which the signal is sufficiently undeformed to estimate the time of arrival using the classical technique of identifying the global peak of the cross-correlation between the emitted and received signals. The

 doi:10.20944/preprints202401.2135.v1

conclusions drawn were that there is a practical limit to the maximum aperture of emitting transducers that can be used in an ultrasonic localization system, and the aperture is smaller as the frequency of the emitted signal increases. Unfortunately, the power of the emitted signal is also proportional to the effective surface area of the transducer, so having a small aperture means limiting the power of the signal and thus limiting the available signal-to-noise ratio (SNR).

In this work, an alternative technique for recognizing the signal's time of arrival is proposed, which also works on strongly aberrated signals. Ultimately, the use of the proposed technique allows the use of larger transducers while maintaining the same spatial coverage and bandwidth of the chirp used, thereby providing a higher SNR. Higher SNRs enable the use of ultrasonic positioning systems in progressively noisier environments, allowing their deployment not only in quiet settings like offices, shops, or hospitals but also in industrial environments.

This paper is structured as follows. Section 2 briefly introduces the simulation tool and setup, while Section 3 focuses on the problem to be addressed. Section 4 presents the proposed technique and the simulation results. Section 5 concludes the paper.

2. Brief introduction to Field II and Simulation Setup

This section provides a concise overview of the operating principle of the Field II simulator [21] and offers a detailed description of the simulation setup. The simulator utilizes spatial impulse responses to model the ultrasound field for pulsed and continuous wave scenarios, employing linear systems theory [23–25]. The spatial impulse response describes the ultrasound field emitted at a specific spatial point over time when the transducer is excited by a Dirac delta function. The overall field generated by any excitation is determined by convolving the spatial impulse response with the excitation function. The technique divides the transducer surface into small rectangles, treating each as a rectangular piston with a known impulsive response [26]. The emitted spherical waves from these elements are then combined to calculate the impulsive responses at each desired field point. This approach allows for flexibility in considering various excitations while maintaining computational efficiency.

In the following simulations, the objective is to investigate the acoustic field and assess the efficacy of the proposed ranging technique within a standard $4 \times 4 \times 3$ m^3 room [27]. Specifically, the simulation results will be carried out for a grid of points forming a vertical section (refer to Section A in the room volume, see Figure 1 in [22]) and a horizontal section positioned midway between the floor and ceiling (refer to Section B in the room volume, Figure 1 in [22]). The transducer, a circular planar one, is centrally positioned on the ceiling at coordinates $x = 0$, $y = 0$, and $z = 0$, emitting downward toward the room floor.

The transducer operates in air, assuming a linearized air absorption model (slope 39.3 dB/m·MHz, constant term -0.262 dB/m, approximately 0.917 dB/m @ 20 kHz, and 1.703 dB/m @ 50 kHz) around 40 kHz. This corresponds to a transducer central frequency of 40 kHz under conditions of 20 °C temperature, 1 atm pressure, and 55% relative humidity [28,29].

The signals emitted and received at various points in the space are influenced by the shape and size of the transducer's emission surface (i.e., aperture D). For this study, a circular plane transducer was selected, possessing similar acoustic properties to widely used transducers in positioning applications, such as the Murata MA40S4S piezoelectric transducer (D = 9.9 mm) or the Pro-wave 328ST/R160 (D = 13.1 mm) [30,31].

Capacitive transducers, on the other hand (e.g., Senscomp models 600 and 7000, etc.), ensure a broader bandwidth but, structurally, have larger apertures ranging from 15 mm to 37 mm. In [22], it was demonstrated that an aperture larger than 8.5 mm does not guarantee the required spatial coverage for indoor positioning applications. Better results were achieved with an aperture as small as 6 mm. Therefore, achieving optimal spatial coverage necessitates a significant reduction in the aperture of these capacitive transducers. However, mechanically reducing the aperture is not well-suited to these transducers and substantially decreases their available acoustic power.

The emitting disk is segmented into a specific quantity of rectangles, specifically square elements measuring 0.125 mm by 0.125 mm in all subsequent simulations. The chosen transducer element size

 doi:10.20944/preprints202401.2135.v1

in this study represents a well-balanced compromise between solution accuracy and the computational resources utilized in the simulation, as shown in Figure 2 in [22].

The signal employed in the simulations is a linear chirp spanning a bandwidth of 30-50 kHz and lasting 5.12 milliseconds [9,27]. For simulation purposes, the signal was sampled at a rate of f_S = 1 MHz. The acoustic field was computed at various points in space throughout a time window aligning with the complete reception duration of the signal [26].

After completing the simulation, the temporal behavior of the acoustic pressure generated by the entire excitation signal was obtained for each considered point in space. This facilitated subsequent assessments and post-processing of the signal, such as calculating peak pressure and total signal strength at each point. Following that, an ideal receiver was assumed, linearly transducing the pressure signal into an electrical signal after suitable sampling and numerical quantization. This process allowed for the calculation of the cross-correlation vector C.

3. Signal aberration

In a previous work [22], the dependence of the signal aberration with the transducer emitting surface area or aperture was shown. The simulations included acoustic diffractive phenomena and frequency-dependent absorption phenomena, as anticipated in the previous section.

In Figure 3 (**c**) in [22], it was shown the results of the estimate of the range obtained using the usual technique based on the search for the position of the cross-correlation peak (τ_{MAX}) [14,32]As a result, for the first four aperture diameters (i.e. 25, 20, 16, and 13.1 mm), the lag of the cross-correlation peak did not correspond to the correct time of arrival (TOA), and the range estimation differed by more than 1.5 cm. It also should be noted that the magnitude of this ranging error is amplified in the subsequent process of spatial coordinate estimation [9].

Further, the impact of using the larger aperture diameter, i.e., D = 25 mm, and the classic ranging technique based on global cross-correlation peak detection in a typical room was illustrated. With this transducer aperture, there was a significant signal shape aberration. However, on the other hand, as expected, the highest power level was achieved, resulting in a higher Signal-to-Noise Ratio (SNR), which is highly desirable in noisy environments.

In Figure 4 (**a**) in [22], the ranging error was evaluated for D = 25 mm. It shows the ranging error along a rectangular vertical section (Section of the room volume, Figure 1) of 3 m height and 4 m base passing through the center of the transducer, equal to the vertical section of the typical office room taken as a reference in some positioning works [27,33], while Figure 7 (**b**) in [22] shows the behavior of the ranging error on a horizontal section of 4 m × 4 m at z = 1.5 m, or halfway between the ground and the ceiling. In both the figures, the grid pitch is 5 cm in the x and y directions.

In this figures, as discussed in [22], it is possible to clearly recognize the low error areas, where the ranging errors are lower than about 3.09 mm. Such ranging error level is due to the numerical approximations and the sampling frequency chosen for the simulation. The simulation results demonstrated that, using the aperture D = 25 mm, therefore, it is not possible to cover the whole room for that height, and things go even worse for higher heights, which, however, are certainly of interest for three-dimensional indoor positioning systems.

4. The signal aberration correction technique

As mentioned earlier, it is highly advantageous to use a transducer with the largest possible emitting surface to achieve high signal intensity and a high Signal-to-Noise Ratio (SNR).

For instance, in Figure 3 (**a**), it can be observed that the acoustic pressure level increases significantly when transitioning from D = 6 mm, which ensures excellent coverage of the entire volume of interest, to D = 25 mm, resulting in a gain of 20 dB on the axis and approximately 15 dB at 90°. However, this larger aperture suffers from substantial ranging errors just outside its emission semi-cone, spanning about 20°.

Therefore, there is a need to develop a new technique that, while preserving the benefits of increased emitted power and SNR with wide apertures, can extend the spatial region where the

 doi:10.20944/preprints202401.2135.v1

ranging error is sufficiently low. In other words, it aims to reduce errors across the entire area of interest.

To achieve this goal, it is insightful to examine the cross-correlation along the same circular path depicted in Figure 1 in [22], namely, along a quarter of a circumference within a plane passing through the transducer's emission axis with a radius of R = 1 m. Figure 1 illustrates the absolute values of cross-correlation amplitudes in dB grayscale, plotted against lag and angle ϑ, for the considered aperture D = 25 mm.

While a well-recognizable cross-correlation peak (white pixels) is evident for ϑ less than 20°, there is a gradual disappearance of a well-defined correlation peak as ϑ increases. There is a double bifurcation at approximately 25° and 54°, complicating the unambiguous identification of the Time of Arrival (TOA).

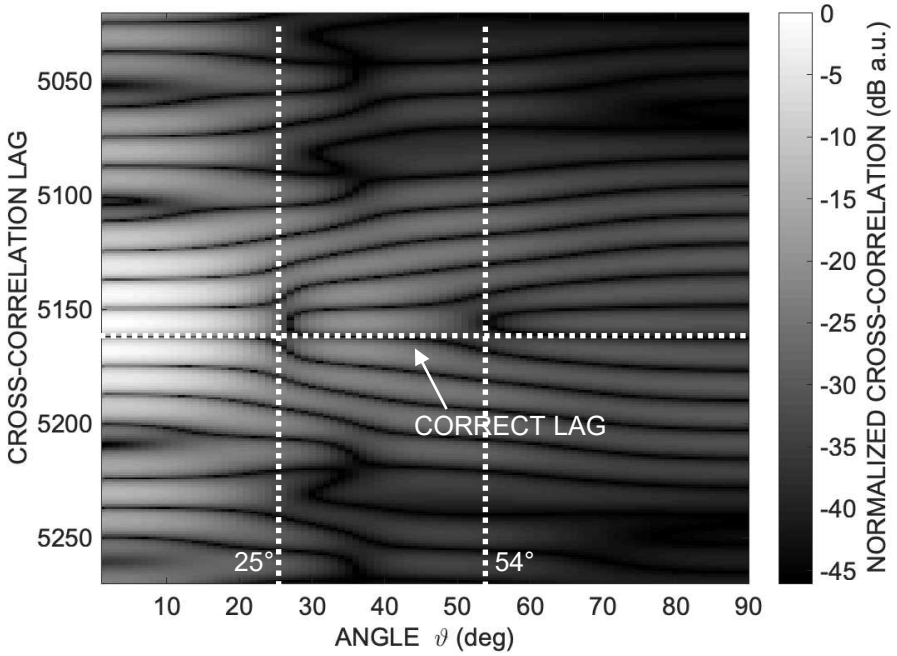

Figure 1. Cross-correlation values along a semicircular path at distance R = 1 m from the emitting transducer and transducer aperture D = 25 mm. It is possible to appreciate the progressive disappearance of a well-defined correlation peak as the angle ϑ increases and a double bifurcation at approximately 25° and 54°, which makes hard the univocal identification of the correct lag and TOA.

Figure 2 displays the cross-correlations along a semicircular path at a distance R = 1 m from the emitting transducer with aperture D = 25 mm at angles out-of-the-axis 0°, 25° and 54°, respectively. In particular, three correlations are shown at 0°, 25° and 54° respectively, which are three columns, represented linearly, of the matrix representing the logarithmic compressed image of Figure 1. The cross-correlations values are normalized to their maximum values. It is possible to appreciate the progressive disappearance of a well-defined single correlation peak as the angle ϑ increases and the appearance of double peaks at the angles of approximately 25° and 54°, in the vicinity of which it is difficult to unambiguously identify the TOA.

 doi:10.20944/preprints202401.2135.v1

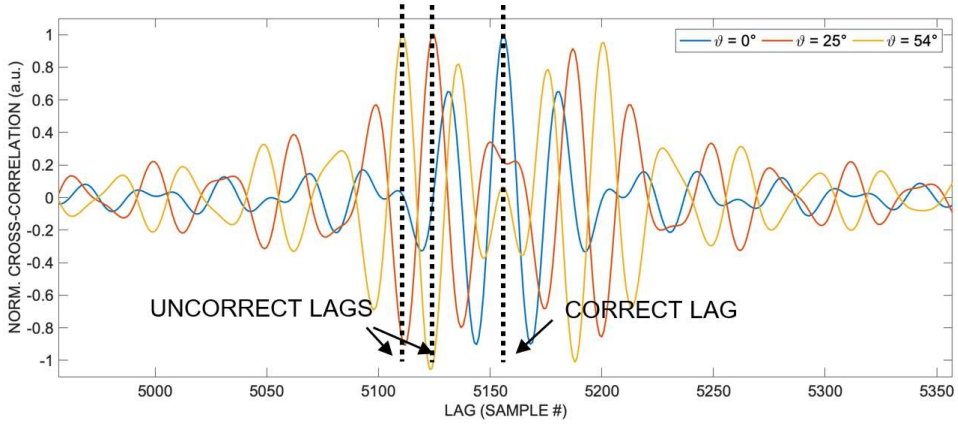

Figure 2. Cross-correlations along a semicircular path at distance R = 1 m from the emitting transducer for the transducer aperture D = 25 mm. It is possible to see that the single unique and well-recognizable peak of the cross-correlation for $\vartheta = 0°$ is no longer present at the 25° and 54° angles. The relative shape deformation with respect to the increasing angle is remarkable and represents a challenge for the correct TOA lag estimation. The cross-correlations values are normalized to their maximum values.

Since the main cause of the increasing error with the angle ϑ from which the transducer is viewed is the self-interference of the acoustic signal from different regions of the same emitting surface of the transducer, which alters the signal shape at the receiver, the underlying idea of the proposed technique is to employ a more sophisticated approach than simple detection of the global peak of the cross-correlation to identify the lag corresponding to the correct Time of Arrival (TOA).

Examining the trend of the cross-correlation in Figure 1 provides a crucial observation. Indeed, it can be observed that at angles around 25° and 52°, the cross-correlation exhibits evident distortion and even a bifurcation in its shape, while elsewhere it remains relatively regular.

These bifurcations underlie the errors in Figure 3 (c) in [22]. More specifically, it is noted that each cross-correlation, despite distorting and losing its unique peak at the correct lag, remains substantially symmetrical around that point, as shown in Figure 2.

This fact suggests the technique proposed here. In fact, considering the points of the cross-correlation falling within a certain amplitude range, for example, with a value exceeding 40% of the global peak, thanks to the symmetry of the waveform, it is possible to estimate the center of this symmetry as the average of the lag for each point weighted with the amplitude of each point, with good approximation. In other words, taking the set of points with values comparable to the global maximum (for example in the range 100% - 40% of the peak value, but of course other choices are possible) of the aberrated cross-correlation, its weighted average has a lag value very similar to that of the global maximum of the undistorted cross-correlation. Hence, it corresponds with good approximation to the correct lag, proportional to the TOA sought.

So, once the signal is received, to estimate the lag corresponding to the Time of Arrival (TOA), it is sufficient to calculate the cross-correlation, take all the points with a value exceeding 40% of the global peak, and compute the weighted average of their lags (see Figure 3).

 doi:10.20944/preprints202401.2135.v1

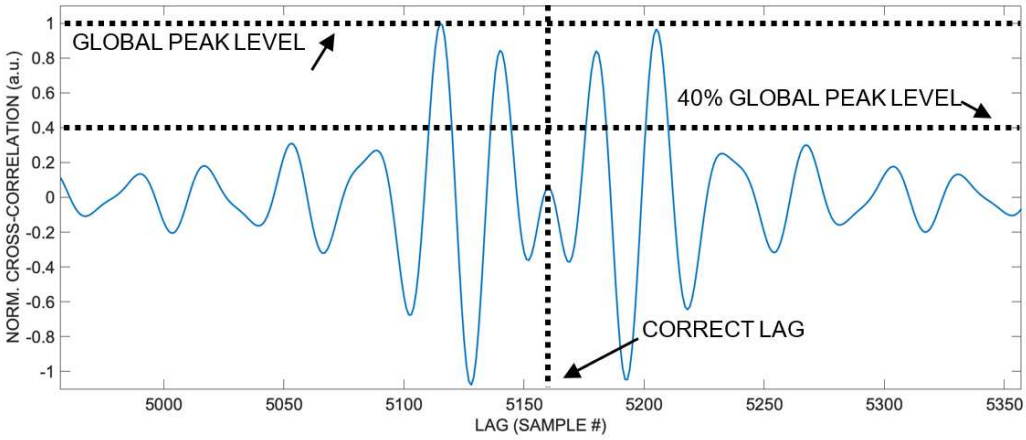

Figure 3. Aberrated cross-correlation shape at $\vartheta = 54°$. Considering cross-correlation values higher than, say, 40% of the global peak, and calculating their weighted average lag, a good approximation of the correct lag is obtained, thanks to the intrinsic symmetry of the cross-correlation.

The following simulations illustrate the results of the procedure described so far. Figure 4 compares the estimated ranges along the circumference of R = 1, obtained by applying the classical cross-correlation global peak detection technique and the proposed weighted averaging lag technique. As is clearly evident, range errors induced by shape aberration are corrected, and the corrected delay can be calculated. The result was of course precisely permitted by the quasi-symmetry of the aberrated cross-correlation.

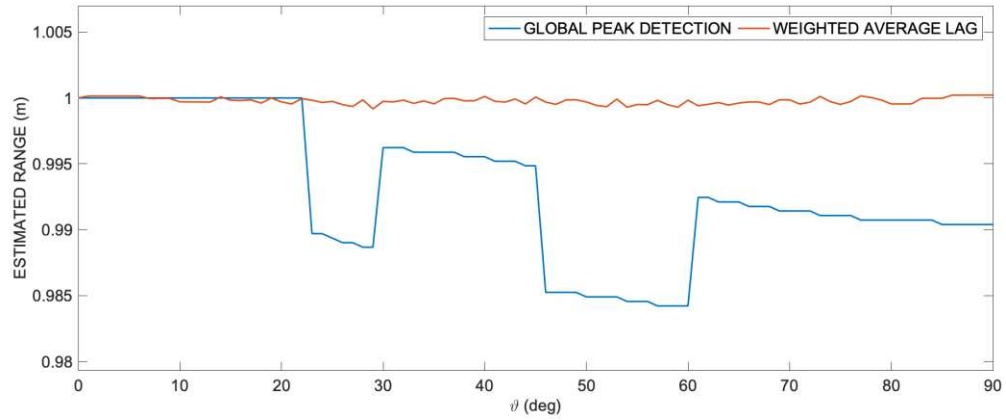

Figure 4. Estimated range comparison between direct detection of the position of the cross-correlation absolute peak and mean lag estimation of the set of the cross-correlation values down to the 40% of the peak value. It is important to notice that the lag of the cross-correlation peak does not allow to estimate the correct range for angles higher than approximately 20°, while the weighted average lag estimation yields a good approximation of the correct range at any angle.

In Figure 5, the estimated range errors for the transducer aperture (D = 25 mm, horizontal and vertical step = 0.05 m) are shown using the technique of weighted average lag on the vertical and horizontal sections of the typical room: (**a**) vertical 4 m × 3 m Section A (see Figure 1 in [22]), where it is noticeable that the cone of minimum ranging error in the vicinity of the transducer axis in the half-space in front of the transducer has disappeared (compare with Figure 6 (**a**) in [22]); (**b**) horizontal 4 m × 4 m Section B, where the disk error pattern present in Figure 7 (**a**) in [22] is absent.

 doi:10.20944/preprints202401.2135.v1

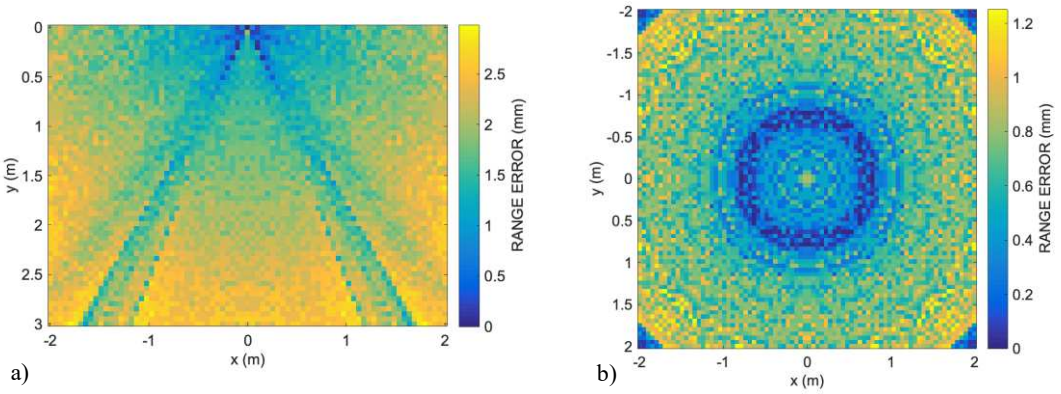

Figure 5. Numerical results for range error using the transducer aperture (D = 25 mm, horizontal and vertical step = 0.05 m) with the weighted average lag technique: (**a**) vertical 4 m × 3 m room section, where the cone of minimum ranging error in the vicinity of the transducer axis in the half-space in front of the transducer has disappeared (compare with Figure 6 (**a**) in [22]); (**b**) horizontal 4 m × 4 m room section, where the disk error pattern present in Figure 7 (**a**) in [22] is absent. The absolute error value is consistently less than 3.0 mm.

5. Conclusions

The article presents a method for correcting signal aberrations in ultrasonic indoor positioning. The challenges associated with signal aberrations in ultrasonic systems, particularly when the aperture of the transducer exceeds a certain limit, causing shape aberrations in the typical linear chirp signal, are addressed. These aberrations impact the cross-correlation technique, leading to errors in range estimation.

To overcome this challenge, the authors propose an alternative technique based on the inherent symmetry observed in the shape of the aberrated cross-correlation. The proposed technique involves calculating the weighted average of lags for points with cross-correlation values exceeding a certain threshold. This method aims to correct the errors introduced by shape aberrations and improve the accuracy of range estimation, allowing for the use of transducers with larger apertures.

The numerical simulations, conducted using the Field II acoustic simulation software, compare the classical cross-correlation technique with the proposed weighted average lag technique in a standard office room. The results demonstrate that the proposed technique enables accurate range estimation even in the presence of severe cross-correlation shape aberrations. This advancement allows for the use of transducers with larger apertures, leading to higher acoustic power and improved Signal-to-Noise Ratio (SNR), and expanding the applicability of ultrasonic systems for indoor positioning and tracking.

Author Contributions: Conceptualization, R.C.; data curation, R.C., M.M., and D.I.; formal analysis, R.C.; investigation, R.C., M.M., D.I.; methodology, R.C.; software, R.C.; supervision, R.C.; writing—original draft, R.C.; and writing—review and editing, R.C., M.M., D.I. All authors have read and agreed to the published version of the manuscript.

Funding: This research received no external funding.

Conflicts of Interest: The authors declare no conflicts of interest.

References

1. Zafari, F.; Gkelias, A.; Leung, K.K. A Survey of Indoor Localization Systems and Technologies. *IEEE Commun. Surv. Tutorials* **2019**, *21*, 2568–2599.
2. Paredes, J.; Álvarez, F.; Aguilera, T.; Villadangos, J. 3D Indoor Positioning of UAVs with Spread Spectrum Ultrasound and Time-of-Flight Cameras. *Sensors* **2017**, *18*, 89.
3. Kunhoth, J.; Karkar, A.; Al-Maadeed, S.; Al-Ali, A. Indoor positioning and wayfinding systems: a survey. *Human-centric Comput. Inf. Sci.* **2020**, *10*, 18.

4. Merenda, M.; Catarinucci, L.; Colella, R.; Iero, D.; Corte, F.G. Della; Carotenuto, R. RFID-based Indoor Positioning using Edge Machine Learning. *IEEE J. Radio Freq. Identif.* **2022**, 1–1.
5. Obeidat, H.; Shuaieb, W.; Obeidat, O.; Abd-Alhameed, R. A Review of Indoor Localization Techniques and Wireless Technologies. *Wirel. Pers. Commun.* **2021**, *119*, 289–327.
6. Seco, F.; Jimenez, A.R.; Prieto, C.; Roa, J.; Koutsou, K. A survey of mathematical methods for indoor localization. In Proceedings of the 2009 IEEE International Symposium on Intelligent Signal Processing; IEEE, 2009; pp. 9–14.
7. Filonenko, V.; Cullen, C.; Carswell, J. Indoor Positioning for Smartphones Using Asynchronous Ultrasound Trilateration. *ISPRS Int. J. Geo-Information* **2013**, *2*, 598–620.
8. Urena, J.; Hernandez, A.; Garcia, J.J.; Villadangos, J.M.; Carmen Perez, M.; Gualda, D.; Alvarez, F.J.; Aguilera, T. Acoustic Local Positioning With Encoded Emission Beacons. *Proc. IEEE* **2018**, *106*, 1042–1062.
9. Carotenuto, R.; Merenda, M.; Iero, D.; Della Corte, F.G. An Indoor Ultrasonic System for Autonomous 3-D Positioning. *IEEE Trans. Instrum. Meas.* **2019**, *68*, 2507–2518.
10. Sabatini, A.M.; Rocchi, A. Sampled baseband correlators for in-air ultrasonic rangefinders. *IEEE Trans. Ind. Electron.* **1998**, *45*, 341–350.
11. Huang, S.S.; Huang, C.F.; Huang, K.N.; Young, M.S. A high accuracy ultrasonic distance measurement system using binary frequency shift-keyed signal and phase detection. *Rev. Sci. Instrum.* **2002**, *73*, 3671–3677.
12. Saad, M.M.; Bleakley, C.J.; Dobson, S. Robust High-Accuracy Ultrasonic Range Measurement System. *IEEE Trans. Instrum. Meas.* **2011**, *60*, 3334–3341.
13. De Marziani, C.; Urena, J.; Hernandez, Á.; Garcia, J.J.; Alvarez, F.J.; Jimenez, A.; Perez, M.C.; Carrizo, J.M.V.; Aparicio, J.; Alcoleas, R. Simultaneous Round-Trip Time-of-Flight Measurements With Encoded Acoustic Signals. *IEEE Sens. J.* **2012**, *12*, 2931–2940.
14. Carotenuto, R.; Merenda, M.; Iero, D.; Della Corte, F.G. Ranging RFID tags with ultrasound. *IEEE Sens. J.* **2018**, *18*, 2967–2975.
15. Carotenuto, R.; Pezzimenti, F.; Corte, F.G. Della; Iero, D.; Merenda, M. Acoustic Simulation for Performance Evaluation of Ultrasonic Ranging Systems. *Electronics* **2021**, *10*, 1298.
16. Rubio, M.C.P.; Serrano, R.S.; Urena, J.U.; Alonso, Á.H.; De Marziani, C.; Franco, F.J.Á. Correlator Implementation for Orthogonal CSS Used in an Ultrasonic LPS. *IEEE Sens. J.* **2012**, *12*, 2807–2816.
17. Jackson, J.C.; Summan, R.; Dobie, G.I.; Whiteley, S.M.; Pierce, S.G.; Hayward, G. Time-of-flight measurement techniques for airborne ultrasonic ranging. *IEEE Trans. Ultrason. Ferroelectr. Freq. Control* **2013**, *60*, 343–355.
18. Kinsler, L.E.; Frey, A.R.; Coppens, A.; Sanders, J. *Fundamentals of Acoustics*; John Wiley & Sons, Inc.: New York, NY, USA, 2000; ISBN 0-471-84789-5.
19. Gualda, D.; Ureña, J.; Jesús García, J.; Jiménez, A.; Pérez, M.C.; Ciudad, F. Coverage analysis of an ultrasonic local positioning system according to the angle of inclination of the beacons structure. In Proceedings of the CEUR Workshop Proceedings; 2019; Vol. 2498, pp. 355–361.
20. Jensen, J.A. FIELD: A program for simulating ultrasound systems. *Med. Biol. Eng. Comput.* **1996**, *34*, 351–352.
21. Field II Ultrasound Simulation Program Available online: https://field-ii.dk/ (accessed on Dec 19, 2023).
22. Carotenuto, R.; Merenda, M.; Iero, D.; G. Della Corte, F. Simulating Signal Aberration and Ranging Error for Ultrasonic Indoor Positioning. *Sensors* **2020**, *20*, 3548.
23. Tupholme, G.E. Generation of acoustic pulses by baffled plane pistons. *Mathematika* **1969**, *16*, 209–224.
24. Stepanishen, P.R. The Time-Dependent Force and Radiation Impedance on a Piston in a Rigid Infinite Planar Baffle. *J. Acoust. Soc. Am.* **1971**, *49*, 841–849.
25. Stepanishen, P.R. Transient Radiation from Pistons in an Infinite Planar Baffle. *J. Acoust. Soc. Am.* **1971**, *49*, 1629–1638.
26. Jensen, J.A.; Svendsen, N.B. Calculation of pressure fields from arbitrarily shaped, apodized, and excited ultrasound transducers. *IEEE Trans. Ultrason. Ferroelectr. Freq. Control* **1992**, *39*, 262–267.
27. Carotenuto, R.; Merenda, M.; Iero, D.; G. Della Corte, F. Mobile Synchronization Recovery for Ultrasonic Indoor Positioning. *Sensors* **2020**, *20*, 702.
28. Bass, H.E.; Sutherland, L.C.; Zuckerwar, A.J.; Blackstock, D.T.; Hester, D.M. Atmospheric absorption of sound: Further developments. *J. Acoust. Soc. Am.* **1995**, *97*, 680–683.
29. García, E.; Holm, S.; García, J.J.; Ureña, J. Link Budget for Low Bandwidth and Coded Ultrasonic Indoor Location Systems. In Proceedings of the International Conference on Indoor Positioning and Indoor Navigation; Guimaraes, Portugal, 2011.
30. Murata Manufacturing Co. Ltd. Specification of Ultrasonic Transducer Type MA40S4S Available online: https://www.murata.com/products/productdata/8797589340190/MASPOPSE.pdf?1450668610000 (accessed on Dec 19, 2023).
31. Pro-Wave Electronic Corp. Air Ultrasonic Ceramic Transducers: 328ST/R160 Available online: http://www.prowave.com.tw/english/products/ut/open-type/328s160c.htm (accessed on Dec 19, 2023).

 doi:10.20944/preprints202401.2135.v1

32. Ens, A.; Reindl, L.M.; Bordoy, J.; Wendeberg, J.; Schindelhauer, C. Unsynchronized ultrasound system for TDOA localization. In Proceedings of the 2014 International Conference on Indoor Positioning and Indoor Navigation (IPIN); IEEE, 2014; pp. 601–610.
33. Medina, C.; Segura, J.; De la Torre, Á. Ultrasound Indoor Positioning System Based on a Low-Power Wireless Sensor Network Providing Sub-Centimeter Accuracy. *Sensors* **2013**, *13*, 3501–3526.